RSC Advances

ROYAL SOCIETY OF CHEMISTRY

www.rsc.org/advances

Journal Name

RSCPublishing

ARTICLE

Evaluation of metal free dye for efficient dye sensitized solar cells based on hydrothermally synthesized TiO_2 nanoflowers

Cite this: DOI: 10.1039/x0xx00000x

Received 00th January 2012,
Accepted 00th January 2012

DOI: 10.1039/x0xx00000x

www.rsc.org/

Chang Su Shim[a], Sawanta S. Mali[a], Ryota Aokie[b], Masski Matsui[b], K. Manseki[c], Chang Kook Hong[a]*

The main aim of the present investigation is to evaluate dye sensitized solar cells (DSSCs) properties of hydrothermally synthesized 3D TiO_2 nanoflower based on DN350 organic dye. The dye loading time has been optimized from the current-voltage (J-V) characteristics in order to get high performance of DSSCs. Further $TiCl_4$ surface treatment was conducted for effective dye loading and fast electron transport for the improvement of DSSCs performance. The perfect optimization of dye loading and its performance evaluation has been optimized and analysed using J-V performance, UV-vis spectroscopy and incident-photon-to-electron conversion efficiency (IPCE) etc. characterization techniques. The diffusion coefficient, diffusion length and electron life time have be evaluated using intensity-modulated photocurrent and photovoltage experiments (IMPS/IMVS). Our optimized results show that, 30min $TiCl_4$ treated TNF samples exhibits current density (J_{SC}) = 14.70mAcm^{-2}, open circuit voltage (V_{OC}) = 0.650V, Fill Factor (FF) = 0.62 with power conversion efficiency (PCE) = 5.92%.

Introduction

Dye-sensitized solar cells (DSSCs) have become one of the most promising alternatives of low-cost photovoltaic technology. Low-cost material, easy fabrication and relatively high conversion efficiency are the promising factors of DSSCs [1]. Mesoporous TiO_2 (mp-TiO_2), light absorber (dyes), iodine based redox electrolyte and catalytic Pt-FTO counter electrodes are key components of DSSCs architecture. The mp-TiO_2, dye loading time and effective catalytic section boost the conversion efficiency. Usually, Ru-based dye requires 24h dye loading time which is needed to the formation of monolayer on metal oxide. However, due to low dietetic constant and low conductivity of organic dyes optimization of dye loading time is strongly influences on its performance. On the other hand, organic dye has much more anchoring sites that facilitate easy adsorption onto metal oxide surface. The small-sized particles suffer from grain boundaries and insufficient light scattering, thus resulting in low light-harvesting efficiency [2]. Moreover, Frank et al. discussed limitations of electron diffusion coefficient and electron collection time in such nanoparticulate samples, which stem mainly from the prevailing hopping mechanism in them [3]. On the other hand, the one dimensional (1D) TiO_2 or ZnO nanostructures could provide slow recombination rate, fast electron transport and effective light scattering ability within the nanostructures. While, 3D nanostructures such as nanoflowers [4], hierarchical microspheres [5] functioning high specific surface area results in an effective dye adsorptive and light-scattering layer. The nanostructures of metal oxides and its composites will open new approaches toward efficient DSSCs. Muduli *et al.* synthesized TiO_2-MWCNT nanocomposite and demonstrated 7.37% PCE using cis-bis(isothiocyanato)bis(2,2'-bipyridyl-4,4'-dicarboxylato)-ruthenium(II) bis-tetrabutylammonium (N-719) dye [6]. On the other hand, Jiang *et al.* developed ZnO-nanoflower array with 1.9% PCE using cis-bis(isothiocyanato)bis(2,2'-bipyridyl-4,4'-dicarboxylato)-ruthenium(II) bis-tetrabutylammonium (N-719) dye. This efficiency has been obtained due to better dye loading and light harvesting of the ZnO-nanoflower structures [7]. To tackle these problems, one dimensional (1-D) growth of nanostructured metal oxides is the effective solution, which can provide a direct path for the rapid collection of photogenerated electrons and reduce the charge recombination. Recently, hierarchical nano/microstructures like hierarchical SnO_2 nanoflowers [8], hierarchical SnO_2 octahedra [9] are used as light-scattering layer with TiO_2 and demonstrated 6.2% and 5.6% power conversion efficiency. Therefore such hierarchical nano/microstructures have attracted much attention in DSSCs owing to the improvement of effective light harvesting, fast transport pathway and effective dye loading. Taking into advantages of hydrothermal technique, we have developed surfactant free hydrothermal synthesis route for 1D as well as 3D TiO_2 nanostructures with well-defined shape and size [2]. Such 1D nanorods arrays with 3D dendrites are provide not only effective surface area but also helpful for effective light harvesting in DSSCs.

It is well known that, ruthenium based dyes are expensive and rare which hampers the cost-effectiveness of DSSCs technology. Therefore metal-free indoline/organic dyes open a unique opportunity towards cost-effective eco-friendly building photovoltaic (BIPV) technology. Recently we have studied variety of organic dyes including DN149, D205, DN319 etc. with mp-TiO_2 and ZnO [10].

To the author's best knowledge there is no single report available based on TiO_2 nanoflowers DN350 organic dye. With this aspect of the limited resources of noble metal, metal-free organic dyes have been introduced for DSSCs [11-13]. The indoline based organic dye D149 was introduced [14] for DSSC with 6.1% conversion efficiency based on the TiO_2. The indoline dye (D205) in which the ethyl group of D149 is substituted with octyl group has been reported to improve the open-circuit voltage (V_{OC}) from the blocking of the charge recombination [13]. The DN319 dye, in which the thiocarbonyl group of D205 in the terminal rhodanine moiety was converted into a dicyanovinylidene unit to achieve higher conversion efficiency than D205 based on the ZnO. Here more bathochromic absorption band plays an important role in fast transportation with good absorption of DN319 dye [15]. The DN350 shows higher conversion efficiency due to bathochromic absorption band and prevention of aggregates formation [15]. In DN350 dye, the 4-(2,2-diphenyvinyliden) phenylene moiety of DN319 is substituted with 2-(9,9-dimethylfluorenyl) group, has been reported to higher efficiency of 5.6% on the ZnO than DN319 due to prevention of aggregates formation of dye elevated by our group [16]. The present study is focused on the evaluation of hydrothermally grown 3D TiO_2 nanoflowers and organic dye DN350 for the DSSCs applications. Initially, hydrothermally grown 3D TiO_2 nanoflowers were treated with $TiCl_4$ and dye loading time has been optimized

2. Experimental

2.1 Methods

Titanium (IV) butoxide ($C1_6H_{36}O_4Ti$) (Aldrich, 97%) (TBT) was dissolved in equal volume of concentrated HCl (37% Sigma Aldrich) and distilled water by magnetic stirring. The fluorine doped tin oxide coated Glass (FTO) substrate was then immersed into the solution parallel to the Teflon wall. The sealed autoclave was then kept in a furnace for 3 h at 180℃. More experimental details are available in our previous report [4]. For the comparison we have used commercial TiO_2 paste (P25, ENB Korea, TTP-20N, ENB-T12010501). The FTO (FTO, Pilkington TEC™ 7Ωcm^{-2}) glasses were washed with soap, water, ethanol and isopropanol each of 15min using the ultrasonication. Commercial TiO_2 (P25) paste was deposited on FTO glass substrate using doctor blade technique (device area 0.25cm^2), and then gradually heated at 550℃ for 10min. The sintered mp-TiO_2 films, as well as hydrothermally grown 3D TiO_2 nanoflower samples, are showing ~8.5μm thickness. For $TiCl_4$ treatment, the deposited TNF and TiO_2 photoelectrodes were immersed in 0.04M $TiCl_4$ solution at 70°C for 30min. After treated samples are gradually heated 550℃ for 10min. The sintered TNF and mp-TiO_2 films are immersed in 0.5mM DN350 dye solution (0.5 mM in a mixture of acetonitrile and tert-butylalchol (v/v, 1:1) with 0.5mM chenodeoxycholic acid) at room temperature. The DN350 organic dye was synthesized as described in the literature [15]. The Pt/FTO counter electrodes were prepared by commercial Pt-paste (Solaronix) as doctor blade technique. The iodide-based electrolyte (Acetonitrile, Valeronitrile (v/v, 85:15) with 0.1M lithium iodide, 0.6M butylmethylimidazolium iodide, 0.05M I_2, 0.05M 4-tert-butylpyriine) [13] was used as the redox electrolyte and injected into the interelectrode space from the counter electrode side through a pre-drilled hole. Dye adsorbed TiO_2 samples are washed with ethanol and dried. For the measurement of dye loading amount, the dried electrodes were immersed in 20ml Dimethyl formamide (DMF, Daujung) solution at 50℃ in 24 h and the dye was totally desorbed in solvent from the electrode.

2.2. Characterizations

The surface morphology of the sample was recorded by a field emission scanning electron microscope (FESEM; S-4700, Hitachi). Transmission electron microscopy (TEM) micrographs, selected area electron diffraction (SAED) pattern and high-resolution transmission electron microscopy (HRTEM) images were obtained by TECNAI F20 Philips operated at 200 KV. The DSSC performances of cells were measured using a solar simulator at AM 1.5 G for 10 s, where the light intensity was adjusted with an NREL-calibrated Si solar cell with a KG-5 filter to 1 sun intensity (100mW.cm^{-2}). The incident-photon-to-current conversion efficiency (IPCE) spectra were measured as a function of wavelength from 300 nm to 800 nm on the basis of a Spectral Products DK240 monochromator. The electron transport time and life time was measured by intensity-modulated photocurrent (IMPS) and photovoltage (IMVS) (Electronic-Chemical Analyzer; Iviumstat, HS technology) with varied the voltage from 0.550 to 1.000V with amplitude from 0.00825 to 0.01500Hz. The dye absorption and dye loading amount on the electrode was measured by UV-vis spectroscopy (Hitachi U-4000, F-4500) range and wavelength. The dye loading amount was measured from desorbed in 20ml Dimethylformamide(DMF, Daujung) solution absorption graph and calculated by a proportional expression from the reference of 0.5M DN350 dye solution of UV absorption peak intensity at 567nm.

3. Results and discussion

3.1. Morphological and structural characterization

Figure 1(a) shows structural representation of an indoline DN350 dye. We have synthesized DN350 dye as per our previous report [16]. Figure 1 (b) shows typical micrograph of mesoporous TiO_2 deposited and sintered on to FTO substrate. The FESEM image shows around 20nm size mesoporous TiO_2 nanoparticles are uniformly deposited throughout the surface. This commercial TiO_2 paste (P25) TTP-20N, ENB-T12010501 was used as a reference electrode. Figure 1 (c) shows surface morphology of TiO_2 nanoflowers (TNF) was synthesized by hydrothermal method. The SEM image shows nanoflowers like morphology having bunch of aligned nanorods. The diameter of nanorod is around 150 to 180nm and total size of nanoflowers is around 2μm as shown in Figure 1 (d). Figure 1 (e) shows spotted SAED pattern indicating single crystalline nature of TiO_2 nanorods. Figure 1 (f) shows highly magnified transmission electron microscopy (TEM) image of the bunch of aligned tetragonal TiO_2nanorods. It is

clear that the nanorods are with 150 nm diameter each nanorod and several micrometer long length has been observed. The agglomerated tetragonal tiny nanorod bundles are separated at the upper side while lower side is compact in nature. It is also notices that, images shows the dendrites are tapered and centered at the core of the nanoflower. The TEM morphology is consistent with FESEM morphology.

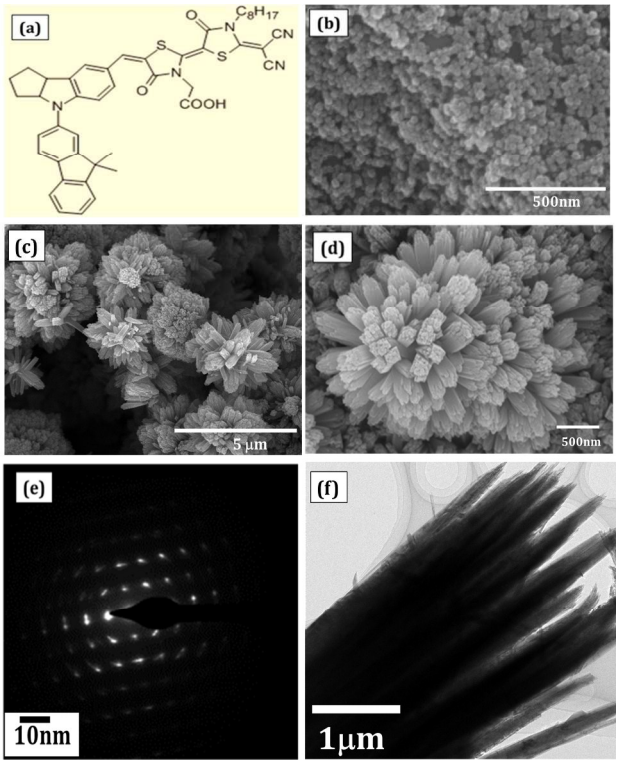

Figure 1 (a) Structural formula of DN350 organic dye, (b) SEM micrograph of mesoporous TiO_2 (P25), (c d) FESEM images of TNF sample at different magnifications (f) SAED pattern (f) HRTEM image of TNF sample

Figure 2 (a) shows typical cross sectional FESEM image of P25 deposited by doctor blade technique. Nearly 8.85µm thick mp-TiO_2 with interconnecting network has been deposited on to FTO substrate. **Figure 2 (b)** shows the XRD pattern of P25 nanoparticles deposited by doctor blade technique. The diffraction peaks of the P25 nanoparticles can be indexed to the pure anatase phase (JCPDS 21-1272). The peaks at 25.49°, 38.16°, 48.07°, 54.69° and 62.79° are ascribed to the reflection of (101), (004), (200) (105), (211), (204) and (220) planes of anatase TiO_2 phase. **Figure 2 (c)** shows typical cross sectional FESEM image of TNF sample. The cross sectional FESEM image shows TiO_2 nanoflowers having uniform size and shape and aligned towards centre to the FTO substrate. The thickness of deposited sample is 9.48 µm. Such type of nanorod arrays are beneficial for effective flow of electrons, effective light harvesting and scattering. **Figure 2 (d)** shows the XRD pattern of TNF sample deposited by hydrothermal route. The diffraction peaks of the TiO_2 nanoflowers can be indexed to the pure rutile phase (021-1276). Eleven distinct reflections such as (110), (101), (200), (111), (210), (211), (220), (002) (310), (301) and (112) are at 27.45, 36.09, 39.21, 41.29, 44.05, 54.32, 56.64, 62.74, 64.05, 69.01 and 69.80, respectively, which show the tetragonal rutile phase of TiO_2. No additional phases were observed.

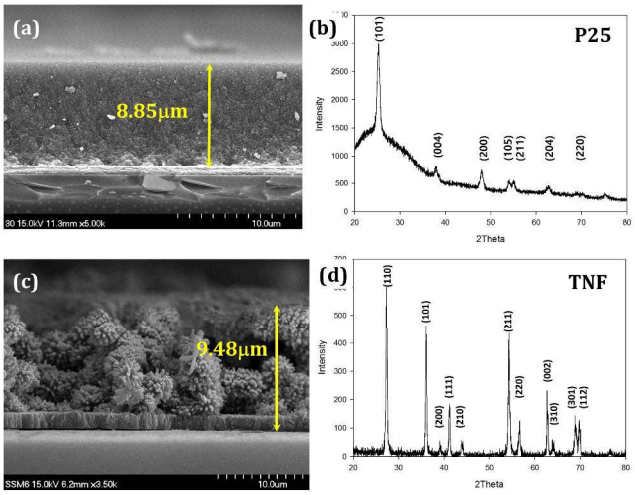

Figure 2 (a & c) Cross sectional FESEM images of P25 and TNF sample. (b & d) show respective XRD patterns.

Figure 3 shows the N2 adsorption–desorption isotherm curves of the P25 and TNF samples. The BET specific surface area of the commercial P25 Degussa powder is 54 m^2g^{-1}. The sample deposited by hydrothemrla route having nanoflower morphology shows 106 m^2g^{-1}, which is much higher than mp-TiO_2 samples. This high surface area is due to the formation of well separated TiO_2 nanorod arrays providing high surface area. These samples facilitates large amount of dye adsorption, fast electron transportation through 1D TiO_2 nanorods, effective light harvesting due to nanorod structure and effective scattering due to nanoflower like morphology [17].

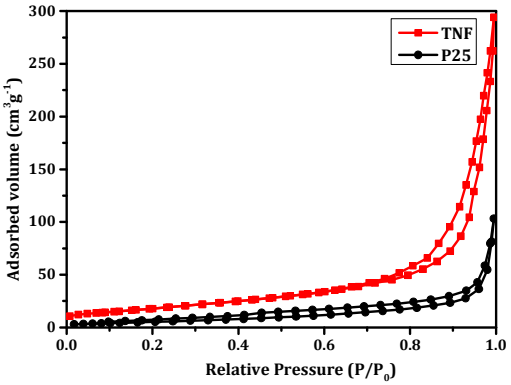

Figure Nitrogen adsorption–desorption isotherms of the commercial P25 and TiO2 nanoflowers deposited by hydrothermal technique.

3.2. Optimization of dye loading time

In DSSCs, dye loading time and formation of monolayer on mesoporous metal oxide is strongly dependent on dye loading concentration, time and anchoring sites. The over

dye loading increases absorption, but recombination rate and device resistance can be increases. Therefore, the optimization of dye loading is a key factor in order to achieve high conversion efficiency with good absorption.

Initially commercially available P25 (ENB-Korea, TTP-20N, Product Name TiO_2 paste (20nm) (TTP-20N), ENB-T12010501.) paste based transparent photoelectrodes were used for dye loading the optimization. The dye loading time was varied from 5 to 90min. **Figure 4** shows the J-V characteristics of DN350 organic dye based on P25 photo electrodes, the dye loading time was varied from 5min, 15min and 90min and measured its J-V plots under 100mWcm^{-2} illumination. The 5min dye loaded sample shows current density (J_{SC}) =6.75mA.cm^{-2}, open circuit voltage (Voc) = 0.660V, fill factor (FF) = 0.61 leading to power conversion efficiency (PCE) η=2.72%. The 15min sample shows Jsc=11.70mA.cm^{-2}, Voc=0.66V, FF=0.62 leading to η=4.79%. Finally 90min dye loading sample shows Jsc=8.62mA.cm^{-2}, Voc=0.660V, FF=0.63 leading to η= 3.58%. From these results it is clear that, 15min dye loading time shows best conversion efficiency (4.79%).

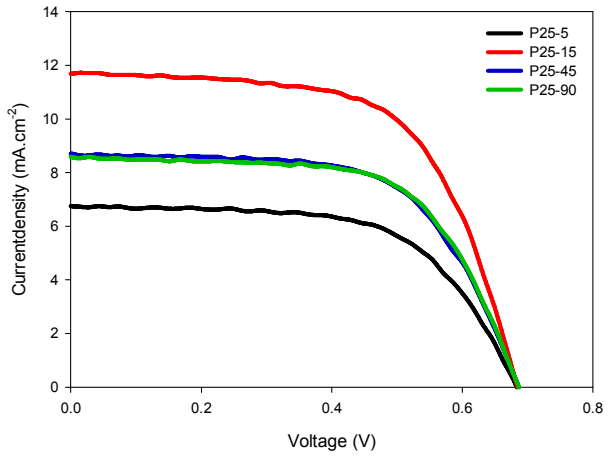

Figure 4 Dye loading time viruses J-V curves based on P25 photoelectrodes.

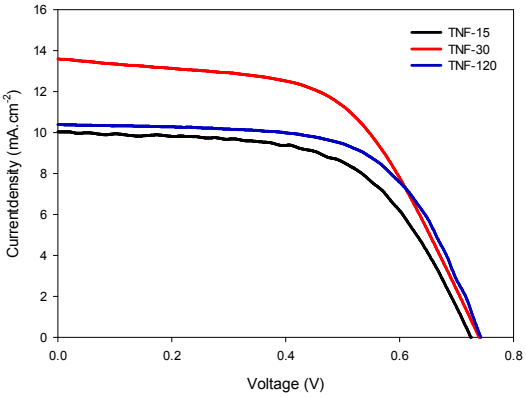

Figure 5 Dye loading time viruses J-V curve based on TNF electrode: TNF-15, TNF-30 and TNF-120 samples for 15 min, 30 min and 120 min respectively.

These optimized conditions were further used for TNF samples. **Figure 5** shows J-V curves for TNF sample with various the dye loading times from 15 to 120 minute. The 15min dye loaded sample shows Jsc=10.04 mA.cm^{-2}, Voc=0.72V, FF=0.59 leading to η= 4.26%. While 30min dye loading time shows the highest performance value of Jsc=13.61 mA.cm^{-2}, Voc=0.730V, FF=0.56 and PEC=5.56%. The over, 120 min dye loading sample shows Jsc=10.39 mA.cm^{-2}, Voc=0.650V, FF= 0.62 leading to η=4.19%. Our 5min and 10min samples show very poor performance for TNF sample. This may happen due to insufficient dye loading. In the present analysis, it is observed that current density for 30min dye loaded sample has been dramatically increased compare to 15min. From this, it is concluded that, 15min dye loading time is enough for TNF sample for sufficient dye loading. Interestingly, it is also observed that 30min sample showed much higher current density than P25-30 min sample. This may be due to efficient dye loading due to high surface area provided by 1D nanostructured TNF which facilitates fast electron transportation.

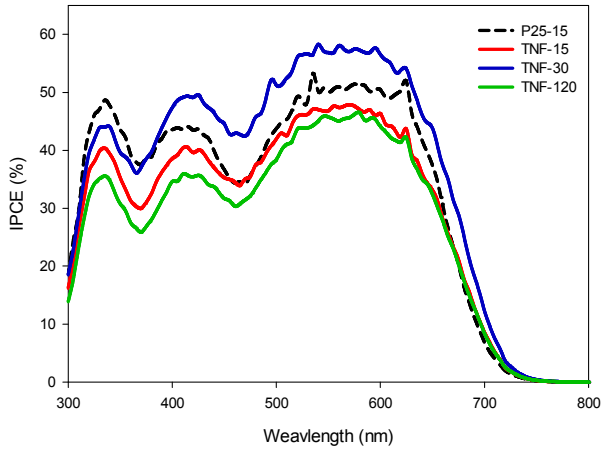

Figure 4 Optimized dye loaded P25 and various dye loading time of TNF samples IPCE spectra.

From above discussion it is clear that, TNF-30 sample shows Jsc=13.61mAcm^{-2}, Voc=0.730V, FF=0.56 and PEC=5.56% which is much higher than P25. In order to evaluate these results, we have recorded the incident-photon-to-electron conversion efficiency (IPCE). **Figure 6** shows the IPCE spectra of optimized dye loaded P25 and various dye loading time of TNF sample in 300-800nm wavelength. All devices show the photocurrent generation start around 730nm in agreement with the band gap of DN350. The IPCE spectra exhibit maximum absorption at approximately 550nm which is highest absorption of DN350 dye. The P25/DN350 sample shows around 50% IPCE while TNF/DN350 sample show 58% IPCE. This means that, dye loading in TNF sample is higher than P25 sample. For the TNF, 30min sample exhibits highest 58% IPCE from 680nm to 530nm wavelength range. On the other hand, TNF 120min photoelectrode shows drastic decrement in IPCE value; it exhibits only 42% IPCE in the respective region. These results concluded that, high dye loading time (120min) hamper the conversion efficiency due to high recombination

rate. It is also observed that TNF 30min shows much higher IPCE value than P25 sample.

The excited electron transferred through the number of grain boundaries in P25 sample. While 1D structure has a lower grain boundaries which facilitates to reduce the recombination compare to P25 [18]. In order to study the electron transport behaviour within these devices, we have recorded the interfacial properties with the help of IMPS/IMVS analysis. **Figure 7** shows the electrodes electron life time, electron transport time and diffusion coefficient for P25 and TNF photoelectrodes. The electron lifetime corresponding to TNF-30 is longer than other all nanofibers may be due to fewer defects. This enables the shorter electron life time and low diffusion coefficient. The diffusion length (Ln) were calculated using following equation $Ln = \sqrt{Dn \times \tau_t}$ [19]. The Ln provides important information regarding electron travelling distance before its recombination. From Ln we can predict the best suitable thickness of photoelectrode for better efficiency.

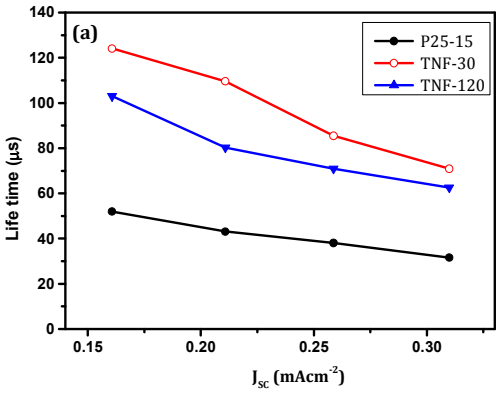

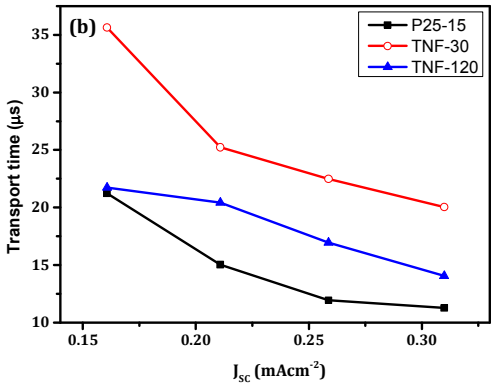

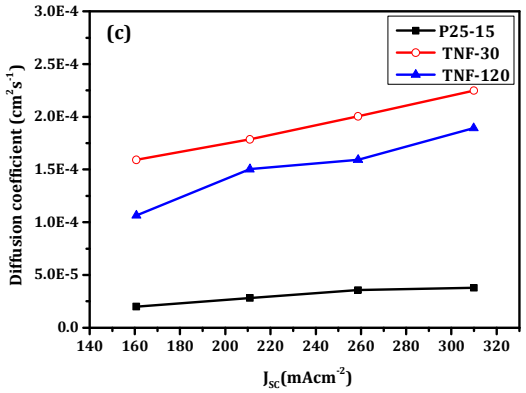

Figure 7 IMPS response of the DSSCs based on P25-15 and TNF-30 photoelectrodes under 0.55 V, 0.70 V, 0.85 V and 1.0 V applied potential. (a) electron lifetimes (τ_e) (b) transport time (τ_t) and (c) Electron diffusion coefficients (Dn) for the P25, TNF-30 and TNF-120 photoelectrodes.

The calculated 'Ln' values are 5.36µm, 5.17µm and 7.56µm for P25, TNF-30 and TNF-120 photoelectrodes respectively. In the present case Ln values were measured for 1V light intensity. The TNF-30 shows lowest Ln value which is one the reason for higher efficiency. From Figure 7 it is clear that, the TNF-30 as well as TNF-120 samples show higher life time compared to P25 photoelectrodes. This may be due to nanoflower morphology of 1D TiO_2 which facilitates scattering within nanoflower architecture. The 1D TiO_2 facilitates fast electron transfer and low recombination rate due to low grain boundaries compared to nanoparticulated TiO_2. From the IMPS/IMVS results, TNF shows higher electron life and short electron transport time than P25. From the above discussion, it is concluded that characters of 1D nanostructure can increase the electron transport property from the dye to FTO for efficient DSSCs.

3.3. $TiCl_4$ treated TNF

In a detailed investigation of dye loading behaviour, we have treated these photoelectrodes to $TiCl_4$ treatment. The $TiCl_4$ treatment is well-known method for the enhancement of the TiO_2 electrode connection can help the increasing the electron transportation. Moreover, it facilitates the downward shift in the band edge and reducing the recombination rate [20-22]. For the improvement of solar cell performance, TNF electrodes were treated with $TiCl_4$ treatment. **Figure 8** shows the J-V plot of $TiCl_4$ treated TNF sample. With respect to different dye loading, the sample TNF 15min exhibits J_{SC}=11.26mA.cm^{-2}, V_{OC}=0.670V, FF=0.60 and PCE =4.53%. The 30min dye loading TNF sample shows J_{SC}=12.27mA.cm^{-2}, V_{OC}=0.670V, FF=0.60 and PCE= 4.93 %. The 120min dye loading TNF sample was showing the highest performance value of J_{SC}=14.70mA.cm^{-2}, V_{OC}=0.650V, FF=0.62 and PCE = 5.92%. Finally the 240min dye loading time TNF sample shows J_{SC}=11.48mA.cm^{-2}, V_{OC}=0.660V, FF=0.56 and PCE=4.24%. The $TiCl_4$ treated TNF the optimized dye loading time showing 120 min in the various dye loading time. Also, the IPCE result showing that the $TiCl_4$ treated TNF showing higher IPCE value than $TiCl_4$ untreated TNF in visual light area. After 120min dye loading time, the IPCE value was decreased.

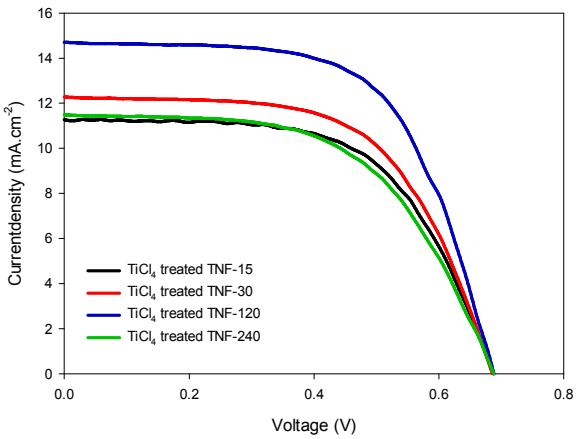

Figure 8 Dye loading time viruses J-V curves of $TiCl_4$ treated TNF electrodes

Figure 9 exhibited detailed spectral formation on the effective light harvesting capability of the samples according to the dye loading time. The IPCE spectrum of DN350 Dye loaded sample shows 63% maximum absorption at approximately 500 to 650 nm, which is attributed to the contribution of effective dye loading samples. The $TiCl_4$ treated sample exhibits 63% IPCE at 567 nm while bare TNF sample shows only 57% IPCE. The IPCE defined terms of the light harvesting efficiency (LHE), electron injection quantum yield (Φ_{inj}) and collection efficiency(η_c) as a followed equation.

$$IPCE = LHE \times \Phi_{inj} \times \eta_c \quad \ldots\ldots \quad (1)$$

The LHE is depending on TiO_2 surface area, dye loading amount and light scattering/reflection factors.

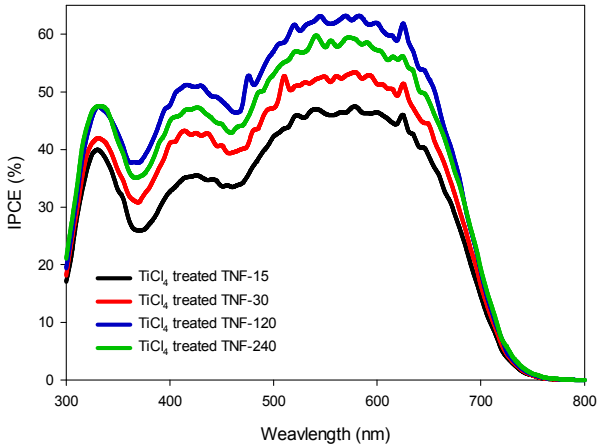

Figure 9 IPCE spectra of various dye loading time of $TiCl_4$ treated TNF photoelectrodes.

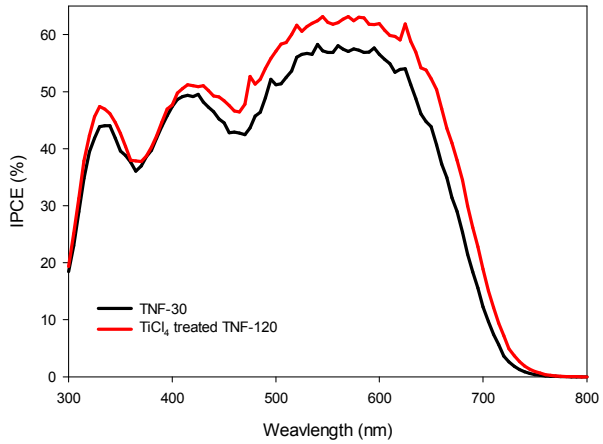

Figure 10 IPCE spectra of optimized bare TNF and $TiCl_4$ treated TNF photoelectrodes. The dye loading time was 30min and 120min for respective samples.

From the **Figure 10** of TNF and $TiCl_4$ treated TNF IPCE spectra, we concluded that the electron injection quantum yield and collection efficiency has been enhanced with the $TiCl_4$ treatment on the TiO_2 nanostructure. **Figure 11** shows UV-vis absorption spectra of $TiCl_4$ treated and untreated sample. The $TiCl_4$ treated and untreated optimized samples from the J-V character, the result shows the initial absorbing speed of the organic dyes was changed. But for the optimized dye loading of each of conditions are showing that similar value from the UV-vis absorption. From the optimized dye loading samples of $TiCl_4$ treated TNF, untreated TNF and untreated P25, dye loading amount was measured by UV-vis spectroscopy in desorbed the solvent. **Table 1** shows that optimized P25 dye loading time at 15min shows the performance value of Jsc=11.70mA.cm^{-2}, Voc= 0.660V, FF=0.62 and PCE=4.79%.

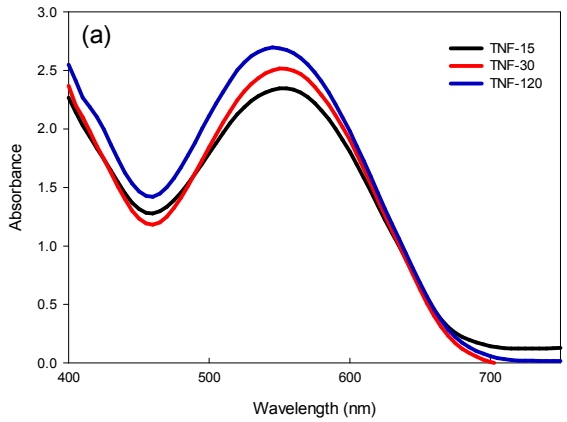

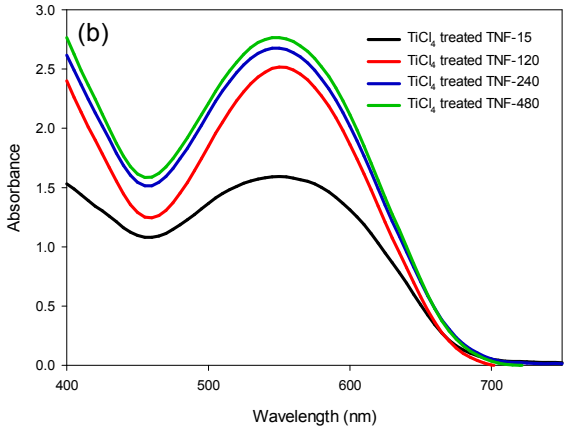

Figure 11 UV-Vis spectra of dye loaded TNF samples with different time interval; (a) without $TiCl_4$ treated (b) $TiCl_4$ treated TNF samples

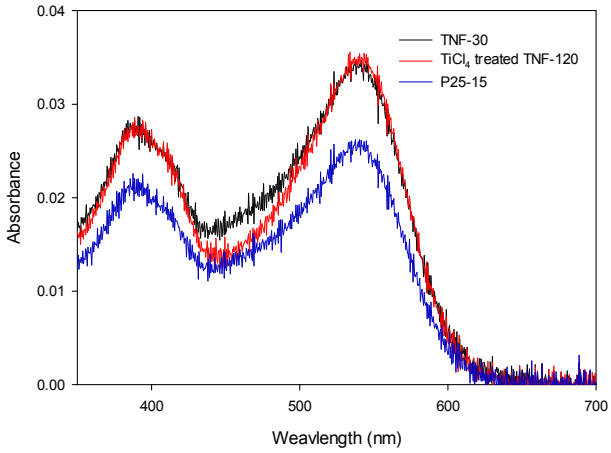

Figure 12 UV-Vis spectra of optimized photoelectrodes used for evaluation of dye loading amount.

Sample	J_{SC} ($mAcm^{-2}$)	V_{OC} (V)	FF (%)	η (%)	Dye loading amount (mol)[b]
P25 -15	11.70±0.25	0.66±0.05	62±1	4.79±0.25	3.2×10^{-4}
TNF-30	13.60±0.20	0.74±0.05	56±1	5.64±0.20	4.2×10^{-4}
$TiCl_4$-TNF-120	14.70±0.20	0.65±0.05	62±1	5.92±0.20	4.3×10^{-4}

Table 1 Average Solar cells performance optimized 20 devices based on P25, TNF and $TiCl_4$ treated TNF photoelectrodes.

The amounts of dye adsorbed of P25-15 photoelectrode (3.2×10^{-4} mol) is lower than that of TNF-30 (4.2×10^{-4} mol) as well as $TiCl_4$-TNF-120 (4.3×10^{-4} mol). From above discussion it is clear that TNF morphology facilitates higher surface area for effective dye loading. On the other hand, $TiCl_4$ treated TNF sample shows small increment in dye loading amount, but the J_{SC} value increased from 13.60 to 14.70$mAcm^{-2}$ results in 5.92% PCE. This may be due to $TiCl_4$ treatment. It is well known that, the $TiCl_4$ treatment is one of the key processes for achieving fast electron transport, low recombination, and dye adsorption. This treatment also reduces grain boundaries and surface traps and better charge carrier separation and hindered recombination [23]. Table 1 concluded the final optimized results for best efficiency based on DN350 for P25 and TNF samples. **Figure 12** shows that optimized dye loaded TNF had more dye loaded than P25. We guess that more dye loaded TNF is from the ability of faster electron transport time and long electron life time of advantage of TNF's 1D structure. After and before $TiCl_4$ treatment of TNF, the optimized dye loading amount was showing the similar amount. Thus our results revealed that, PCE for DN350 is $TiCl_4$-TNF-120 > TNF-30 >$TiCl_4$-mp-TiO_2 > mp-TiO_2. However, the dye loading time is different for each photoelectrodes.

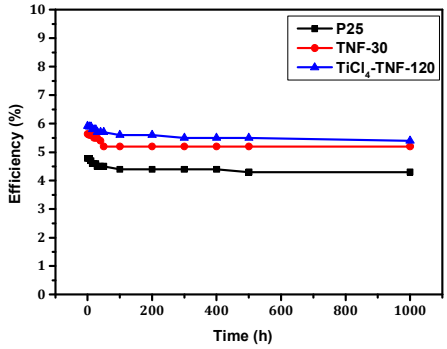

Figure 13 Stability of optimized devices based on P25, TNF-30 and $TiCl_4$-TNF-120 photoelectrodes.

In order to check the stability of these devices, we have tested life time stability performance of these devices of respective condition and recorded its performance. For stability testing, the fabricated devices were stored in dark before and after measurements. **Figure 13** shows the stability performance up to 1000h. Overall, all devices shows air good stability up to 500h while little decrement has been observed later.

4. Conclusions

We have optimized the DN350 dye loading parameters for commercial P25 and hydrothermally grown TNF samples. The 15min for P25 and 30min for bare 3D TNF is enough for sufficient dye loading, and these samples exhibited 4.79% and 5.56% conversion efficiency respectively. While, $TiCl_4$ treated sample exhibit 15min for P25 photoelectrodes and 120min for TNF photoelectrodes dye loading exhibits excellent power conversion efficiency 5.56% and 5.92% respectively. The prepared 3D TNF sample offers much higher surface area and excellent charge separation results in high solar cell performance. The thicker photoelectrodes will also be improved conversion efficiency. This study is underway in our laboratory.

Acknowledgements

This study was financially supported by Chonnam National University, 2010. This research was also supported by Basic Science Research Program though the National Research

Foundation of Korea (NRF) funded by the Ministry of Education (NRF-2009-0094055)

Notes and references

[a]*Department of Chemical Engineering, Chonnam National University, Gwangju South Korea, 500-757, Email: hongck@chonnam.ac.kr*
[b]*Department of Materials Science and Technology, Faulty of Engineering, Gifu University, Yanagido, Gifu Japan, 501-1193,*
[c]*Graduate School of Engineering, Environmental and Renewable Energy System (ERES) Division, Gifu University, Yanagido, Gifu Japan, 501-1193,*

[1] B. O'Regan and M. Grätzel *Nature* 1991,**353,** 737.
[2] G. Schlichthorl, N.G. Park, A.J. Frank, *J. Phys. Chem. B* 1999, **103,** 782.
[3] S. S. Mali, R. S. Devan, Y.-R. Ma, C. A. Betty, P. N. Bhosale, R. P. Panmand, B. B. Kale, S. R. Jadkar, P. S. Patil, J. –H. Kim, C. K. Hong, *Electrochimica Acta* 2013, 90, 666– 672
[4] S. S. Mali, H. Kim, S. Shim, P. S. Patil, J. H. Kim and C. K. Hong. *Sci Rep.,* 2013, **3,** 3004.
[5] Mali, S. S., Betty, C. A., Bhosale, P. N. and Patil, P. S. *CrystEngComm,* 2011, **13,** 6349–6351.
[6] S. Muduli, W. Lee, V. Dhas, S. Mujawar, M. Dubey, K. Vijayamohanan, S. –H.Han, and S. Ogale, *ACS Appl. Mater. Interface,* 2009, 1, 2030-2035.
[7] C. Y. Jiang, X. W. Sun, G. Q. Lo, and D. L. Kwong, Appl. Phys. Lett. 2007, 90, 263501.
[8] H. Niu, S. Zhang, R. Wang, Z. Guo, X. Shang, W. Gan, S. Qin, L. Wan and J. Xu, *J. Phys. Chem. C* 2014, 118, 3504-3513
[9] Y.-F. Wang, J.-W. Li, Y. –F. Hou, X.-Y. Yu, C.-Y. Su, and D.-B. Kuang, *Chem. Eur. J.* 2010, 16, 8620-8625
[10]M. Matsui, M. Ono, Y. Kubota, K. Funabiki, T. Yoshida, H. Jin Kim, C. K. Hong, S. Higashijima and H. Miura, Dyes and Pigments 2013, **99**, 829-832
[11] Z. Tian, M. Huang, B. Zhao, H. Huang, X. Feng, Y. Nie, P. Shen and S. Tan, *Dyes Pigm*., 2010**, 87**, 181-187.
[12] N. Koumura, Z.-S. Wang, M. Miyashita, Y. Uemura, H. Sekiguchi, Y. Cui, A. Mori, S. Mori and K. Hara, *J. Mater. Chem*., 2009, **19**, 4829–4836.
[13] S. Ito, Hidetoshi Miura, S. Uchida, M. Takata, K. Sumioka, P. Liska, P. Comte, P. Péchy and M. Grätzel, *Chem. Commun.,*2008, 5194-5196
[14] T. Horiuch, H. Miura, S. Uchida, *Chem. Commun.,*2003, 3036-7.
[15] S. Higashijima, H. Miura, T. Fujita, Y. Kubota, K. Funabiki, T. Yoshida, M. Matsui, *Tetrahedron*, 2011, **67**, 6289-6293
[16] S. Higashijima, Y. Inoue, H. Miura, Y. Kubota, K. Funabiki, T. Yoshida, M. Matsui, *RSC Adv.,* 2012, 2721-2724.
[17] S. S. Mali, H. J. Kim, C. S. Shim, W. R. Bae, N. L. Tarwal, S. B. Sadale, P. S. Patil, J.-H. Kim and C. K. Hong, *CrystEngComm,* 2013, **15**, 5660-5667
[18] Y. H. Jung, K. H. Park, J. S. Oh, D. H. Kim and C. K. Hong, *Nanoscale Res. Lett.,* 2013, **8**, 37
[19] J. Y. Kim, J. H. Noh, K. Zhu, A. F. Halverson, N. R. Neale, S. Park, K. S. Hong and A. J. Frank, *ACS Nano* 2011, **5,** 2647−2656.
[20] G. O. Kim, K. W. Kim, K. K. Cho and K. S. Ryu. *Appl. Chem. Eng.,* 2011, **22**, 2, 190-195
[21] J. K. Kim, K. Shin, K. S. Lee and J. H. Park. *J. Electrochem. Sci. Tech.* 2010, **1**, 2, 81-84
[22] P. M. Sommeling, B. C. O'Regan, R. R. Haswell, H. J. P. Smith, N. J. Bakker, J. J. T. Smits, J. M. Kroon, and J. A. M. van Roosmalen, *J. Phys. Chem. B* 2006**, 110,** 19191-19197
[23] S. S. Mali, C. S. Shim, H. K. Park, J. Heo, P. S. Patil and C. K. Hong, *Chem. Mater.* 2015, **27,** 1541−1551

